Inorganic Chemistry
Article

Inorg. Chem. **2010**, *49*, 7353–7361 **7353**
DOI: 10.1021/ic1004769

New Iridathiaboranes with Reversible *Isonido* ↔ *Nido* Cluster Flexibility

Jonathan Bould,*,† Carmen Cunchillos,§ Fernando J. Lahoz,§ Luis A. Oro,‡,§ John D. Kennedy,∥ and Ramón Macías*,‡

†*Institute of Inorganic Chemistry of the Academy of Sciences of the Czech Republic, 250 68 Husinec-Řež 1001, Czech Republic,* ‡*Departamento de Química Inorgánica, Instituto Universitario de Catálisis Homogénea, and* §*Instituto de Ciencia de Materiales de Aragón, Universidad de Zaragoza-Consejo Superior de Investigaciones Científicas, 50009-Zaragoza, Spain, and* ∥*School of Chemistry of the University of Leeds, Leeds LS2 9JT, U.K.*

Received March 12, 2010

The reaction between $[IrCl(CO)(PMe_3)_2]$ and the Cs[*arachno*-6-SB_9H_{12}] salt in CH_2Cl_2 yields pale-yellow 11-vertex [8,8,8-$(CO)(PMe_3)_2$-*nido*-8,7-$IrSB_9H_{10}$] (**4**). Reaction of this CO-ligated iridathiaborane with $Me_3N{=}O$ affords pale-yellow 11-vertex [1,1,1-$(H)(PMe_3)_2$-*isonido*-1,2-$IrSB_9H_9$] (**6**), which is also formed from the thermal decarbonylation of **4**. Compound **4** has a conventional cluster structure based on classical 11-vertex *nido* geometry, with the iridium center and the sulfur atom in the adjacent 8- and 7-positions on the pentagonal open face. Compound **6** exhibits an 11-vertex *isonido* structure based on an octadodecahedron with the $\{Ir(H)(PMe_3)_2\}$ occupying the apical position of connectivity six, but with one long non-bonding Ir−B distance generating the quadrilateral *isonido* open-face. Compound **6** reverts to **4** upon reaction with CO, and the Lewis acid character of **6** is further demonstrated in the reaction with EtNC to give [8,8,8-$(EtNC)(PMe_3)_2$-*nido*-8,7-$IrSB_9H_{10}$] (**7**). The three new compounds **4**, **6**, and **7** have been characterized by single-crystal X-ray diffraction analyses and by NMR spectroscopy. Each of the *nido* iridathiaboranes **4** and **7** exhibits two different $\{Ir(L)(PMe_3)_2\}$-to-$\{SB_9H_{10}\}$ conformers in solution and in the solid state. Density functional theory (DFT) calculations reveal that the iridium atom inverts the *nido*-*isonido*-*closo* energy profile previously found for the rhodathiaborane congener [8,8,8-$(PPh_3)_2$-*nido*-8,7-$RhSB_9H_{10}$] (**3**), demonstrating how the structure of these 11-vertex clusters can be controlled and fine-tuned by the tailoring of the metal center.

Introduction

The multiple chemical processes in which transition-element complexes and boranes combine to functionalize hydrocarbons, or to produce dihydrogen from aminoboranes, generally involve σ-interactions with borane and alkane molecules.[1−3] These types of interaction lead to the activation of B−H and C−H bonds, which may then result in the formation of intermediates that exhibit M-η^2-(H−E) bonds and/or M−E σ-bonds, where E = B and/or C.[4,5] Thus, compounds that contain metal and boron, and that can combine these kinds of bonds in their structure, are good models for the study of C−H and B−H activation reactions that finally lead to the formation of C−B bonds in hydrocarbons or to the production of dihydrogen from aminoboranes.[6−9]

Metallaboranes and metallaheteroboranes are polyhedral compounds that exhibit M−B and also, often, M−H−B bonds, and these compounds are expected to possess aspects of reactivity associated with both the metal and the borane fragments.[10−12] In addition, however, with these polyhedral cluster species, reaction properties associated with the cluster bonding network can contribute decisively to observed reactivities. Among such species, reversible *nido*-to-*closo* transformations coupled with hydrogen transfer to organic substrates have been found to open new mechanisms for the functionalization of organic molecules in catalytic cycles.[13−17]

*To whom correspondence should be addressed. E-mail: rmacias@unizar.es (R.M.), jbould@gmail.com (J.B.).

(1) Brown, H. C. *Hydroboration*; Benjamin: New York, 1962.
(2) Chen, H.; Schlecht, S.; Semole, T. C.; Hartwig, J. F. *Science* **2000**, *287*, 1995–1997.
(3) Baker, T. R. *Dalton Trans.* **2007**, 2613–2626.
(4) Perutz, R. N.; Sabo-Etienne, S. *Angew. Chem., Int. Ed.* **2007**, *46*, 2578–2592.
(5) Alcaraz, G.; Grellier, M.; Sabo-Etienne, S. *Acc. Chem. Res.* **2009**, *42*, 1640–1649.
(6) Waltz, K. M.; Hartwig, J. F. *J. Am. Chem. Soc.* **2000**, *122*, 11358–11369.
(7) Douglas, T. M.; Chaplin, A. B.; Weller, A. S.; Yang, X.; Hall, M. B. *J. Am. Chem. Soc.* **2009**, *131*, 15440–15456.
(8) Denney, M. C.; Pons, V.; Hebden, T. J.; Heinekey, D. M.; Goldberg, K. I. *J. Am. Chem. Soc.* **2006**, *128*, 12048–12049.
(9) Chaplin, A. B.; Weller, A. S. *Angew. Chem., Int. Ed.* **2010**, *49*, 581–584.
(10) Fehlner, T. P. *Organometallics* **2000**, *19*, 2643–2651.
(11) Kennedy, J. D. *Prog. Inorg. Chem.* **1984**, *32*, 519–679.
(12) Kennedy, J. D. *Prog. Inorg. Chem.* **1986**, *34*, 211–434.
(13) Álvarez, A.; Macías, R.; Bould, J.; Cunchillos, C.; Lahoz, F. J.; Oro, L. A. *Chem.—Eur. J.* **2009**, *15*, 5428–5431.
(14) Álvarez, A.; Macías, R.; Fabra, M. J.; Lahoz, F. J.; Oro, L. A. *J. Am. Chem. Soc.* **2008**, *130*, 2148–2149.

Published on Web 07/21/2010

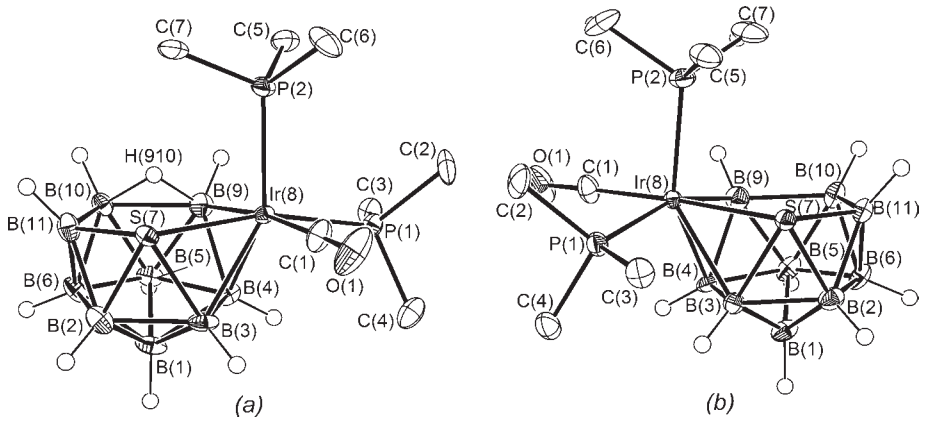

Figure 1. ORTEP-type representations of (*a*) the major (84%) and (*b*) the minor (16%) occupancy conformers in crystals of [8,8,8-$(PMe_3)_2$(CO)-*nido*-8,7-$IrSB_9H_{10}$] (**4**); 50% probability ellipsoids. Hydrogen atoms on the PMe_3 ligands are omitted to aid clarity. The hydrogen atom in B(9)−H−B(10) (b) was not located for the minor conformer.

Although the existing results from these types of systems are significant, very few instances of reversible stoichiometric reactions or catalytic cycles that involve metallaboranes or metallaheteroboranes have been published.[18−20] Within this context, we have recently reported reversible dihydrogen activation using the 11-vertex rhodathiaborane system consisting of [8,8,8-$(PPh_3)_2$(H)-*nido*-8,7-$RhSB_9H_9$-9-(NC_5H_5)] (**1**) and [1,1-$(PPh_3)_2$-*closo*-1,2-$RhSB_9H_8$-3-(NC_5H_5)] (**2**),[14] which, under catalytic conditions, is active in hydrogenations of alkenes.[15]

In addition, the reported reaction chemistry of iridaboranes with small unsaturated organic molecules suggests that there is a considerable potential for the development of organometallic chemistry based on clusters that incorporate iridium vertices. For example, the reaction of the *nido*-6-iridadecaborane [6-(PPh_3)-μ-6^P,5^C-(Ph_2P-*ortho*-C_6H_4)-6-H-*nido*-6-IrB_9H_{12}] with acetylene affords [μ-1^C,2^P-(Ph_2P-*ortho*-C_6H_4)-2,2-$(PH_3)_2$-*closo*-2-IrB_9H_7-10-(PPh_3)] and [μ-1^P,2^C-(Ph_2P-*ortho*-C_6H_4)-1,1-(C_4H_4)-*closo*-1-IrB_9H_8-6-(PPh_3)]. In the former, the PPh_3 ligands have been converted to PH_3 ligands and the cluster oxidized from *nido* to *closo*; whereas in the latter, two acetylene groups have dimerized to form an iridacyclopenta-2,4-dienyl moiety, and the cluster is transformed from *nido* to *closo*.[21]

The reactivities of these rhodathiaboranes and iridaboranes are a consequence of the combined and synergic redox flexibilities of both the clusters and the transition-element centers: together they enable a reversible *nido*-to-*closo* transformation coupled to either the dihydrogen release or the transfer of hydrogen atoms from the boron part of the cluster to unsaturated molecules. Given the interesting results arising from these systems,[13−15,21] we decided to examine the possibility that the chemistry of the rhodium-containing borane cluster compounds might be both mirrored and modified by the use of analogous or otherwise related iridium species.

Consequently, here we now report the preparation of a new iridathiaborane that arises from the reaction of the [*arachno*-6-SB_9H_{10}]$^-$ anion with the iridium complex [IrCl(CO)$(PMe_3)_2$], the product of its chemical decarbonylation, and also a new EtNC-ligated iridathiaborane. When compared with the rhodathiaborane counterparts, the new iridathiaboranes exhibit significant structural and spectroscopic differences that augur well for a rich reaction chemistry that may ultimately complement and extend that discovered for the rhodathiaborane **1**/**2** system.

Results and Discussion

The principal synthetic route to metallaboranes and metallaheteroboranes is to add metal fragments to preformed borane and heteroborane species. As the borane or heteroborane framework is quite robust, the majority of products contain a single metal center, and very often the result is a cluster with an additional vertex.[22−24] This synthetic approach has been particularly convenient in the preparation of 11-vertex *nido*-metallaheteroboranos of general formulation, [8,8-$(L)_2$-*nido*-8,7-MEB_9H_{10}], where M is Rh, L is PPh_3, and E is S, CH, or NH; and where M is Pt, L is PMe_2Ph, and E is CH.[25−27] These last species are all formally unsaturated according to the Wade−Williams cluster-geometry electron-counting paradigm,[28,29] with the "unsaturation" arising from the tendencies of rhodium and platinum to adopt square-planar

(15) Álvarez, A.; Macías, R.; Bould, J.; Fabra, M. a. J.; Lahoz, F. J.; Oro, L. A. *J. Am. Chem. Soc.* **2008**, *130*, 11455–11466.
(16) Behnken, P. E.; Belmont, J. A.; Busby, D. C.; Delaney, M. S.; King, R. E.; Kreimendahl, C. W.; Marder, T. B.; Wilczynski, J. J.; Hawthorne, M. F. *J. Am. Chem. Soc.* **1984**, *106*, 3011–3025.
(17) Hong, Y. B.; A. M.; Fehlner, T. P. *Organometallics* **2002**, *21*, 5029–5037.
(18) Kadlecek, D. E.; Carroll, P. J.; Sneddon, L. G. *J. Am. Chem. Soc.* **2000**, *122*, 10868–10877.
(19) Littger, R.; Englich, U.; Ruhlandt-Senge, K.; Spencer, J. T. *Angew. Chem., Int. Ed.* **2000**, *39*, 1472–1474.
(20) Macías, R.; Fehlner, T. P.; Beatty, A. M. *Angew. Chem., Int. Ed.* **2002**, *41*, 3860–3862.
(21) Bould, J.; Bown, M.; Coldicott, R. J.; Ditzel, E. J.; Greenwood, N. N.; Macpherson, I.; MacKinnon, P.; Thornton-Pett, M.; Kennedy, J. D. *J. Organomet. Chem.* **2005**, *690*, 2701–2720.
(22) Barton, L., Strivastava, D. K. In *Comprehensive Organometallic Chemistry II*; Abel, E. W.; Stone, F. G. A., Wilkinson, G., Eds.; Pergamon: New York, 1995; Vol. *1*.
(23) Weller, A. S. In *Comprehensive Organometallic Chemistry*; Crabtree, R. H., Mingos, D. M. P., Eds.; Elsevier: Oxford, 2007; Vol. *3*, Chapter 3.04, pp 133−174.
(24) Wesemann, L. In *Comprehensive Organometallic Chemistry*; Crabtree, R. H., Mingos, D. M. P., Eds.; Elsevier: Oxford, 2007; Vol. *3*, Chap. 3.03, p 113.
(25) Ferguson, G.; Jennings, M. C.; Lough, A. J.; Coughlan, S.; Spalding, T. R.; Kennedy, J. D.; Fontaine, X. L. R.; Štíbr, B. *J. Chem. Soc., Chem. Commun.* **1990**, 891–894.
(26) Štíbr, B.; Jelinek, T.; Kennedy, J. D.; Fontaine, X. L. R.; Thornton-Pett, M. *J. Chem. Soc., Dalton Trans.* **1993**, 1261–1267.
(27) Macías, R.; Bould, J.; Holub, J.; Kennedy, J. D.; Štibr, B.; Thornton-Pett, M. *Dalton Trans.* **2007**, 2885–2897.
(28) Wade, K. *Inorg. Nucl. Chem. Lett.* **1972**, *8*, 559–566.
(29) Williams, R. E. *Inorg. Chem.* **1971**, *10*, 210–214.

Table 1. Selected Interatomic Distances (Å) for $[(PMe_3)_2(CO)$-*nido*-$IrSB_9H_{10}]$ **4**, $[(PMe_3)_2(EtNC)$-*nido*-$IrSB_9H_{10}]$ **7**, and $[(PMe_3)_2H$-*isonido*-$IrSB_9H_9]$ **6**[a]

	4 [**4a**]	**7**		**6**
Ir(8)−S(7)	2.4026(17) [2.4600]	2.400(2)	Ir(1)−S(2)	2.396(3)
Ir(8)−P(1)	2.3119(14) [2.3234]	2.305(2)	Ir(1)−P(1)	2.340(2)
Ir(8)−P(2)	2.3433(15) [2.3781]	2.353(2)	Ir(1)−P(2)	2.311(2)
Ir(8)−C(1)	1.909(5) [1.945]	2.003(8)	Ir(1)−B(3)	2.122(13)
Ir(8)−B(3)	2.263(6) [2.322]	2.271(9)	Ir(1)−B(4)	2.779(9)
Ir(8)−B(4)	2.250(6) [2.287]	2.235(8)	Ir(1)−B(5)	2.388(9)
Ir(8)−B(9)	2.273(16) [2.310]	2.35(3)	Ir(1)−B(6)	2.377(8)
S(7)−B(2)	1.975(6) [1.998]	1.989(11)	Ir(1)−B(7)	2.396(8)
S(7)−B(3)	2.090(6) [2.197]	2.130(10)	S(2)−B(4)	1.900(9)
S(7)−B(11)	1.909(6) [1.922]	1.944(9)	S(2)−B(5)	1.981(10)
B(9A)−B(10) (longest)	1.898(16) [1.873]	1.96(2)	S(2)−B(8)	2.012(9)
B(6)−B(11) (shortest)	1.733(8) [1.730]	1.746(14)	B(5)−B(8) (longest)	1.888(13)
B−B (average)	1.7845(14)	1.800(9)	B(3A)−B(9) (shortest)	1.689(17)
C(1)−O(1)/N(1)	1.130(8) [1.151]	1.152(10)	B−B (average)	1.787(13)
P(1)−Ir(8)−P(2)	97.90(5) [98.19]	97.43(7)	P(1)−Ir(1)−P(2)	102.48(7)
P(1)−Ir(8)−S(7)	165.68(5) [164.14]	166.44(15)	P(1)−Ir(1)−S(2)	98.96(10)
P(2)−Ir(8)−S(7)	96.28(5) [96.75]	95.71(15)	P(2)−Ir(1)−S(2)	96.21(9)
P(1)−Ir(8)−B(9)	94.6(4) [89.95]	92.9(4)	P(1)−Ir(1)−B(3)	109.1(3)
P(2)−Ir(8)−B(9)	89.37.8(3) [83.33]	92.0(5)	P(2)−Ir(1)−B(3)	128.1(3)
S(7)−Ir(8)−B(9)	87.4(4) [86.55]	90.0(5)	S(2)−Ir(1)−B(3)	117.5(4)

[a] Corresponding calculated distances for the model compound, $[(PH_3)_2(CO)$-*nido*-$IrSB_9H_{10}]$ **4a** are enclosed [in brackets]. The model corresponds to the higher occupancy conformer.

16-electron metal configurations.[27,30] Thus, treatment of Cs[*arachno*-6-SB_9H_{12}][31] with the Wilkinson catalyst [RhCl-$(PPh_3)_3$][32] affords the 11-vertex rhodathiaborane [8,8-$(PPh_3)_2$-*nido*-8,7-$RhSB_9H_{10}$] (**3**) in high yield and allows the systematic study of its chemistry.[25]

In contrast, the reactions of the thiaborane anion $[SB_9H_{12}]^-$ with the iridium analogue of Wilkinson's catalyst, $[IrCl(PPh_3)_3]$, or with Vaska's compound, $[IrCl(CO)(PPh_3)_2]$, have been reported not to result in the incorporation of the corresponding iridium fragment into the cluster framework.[33] We surmised that the PMe_3 ligated analogues of these chloride compounds might behave differently. The PMe_3 analogue of Wilkinson's complex, $[IrCl(PMe_3)_3]$, has been reported to be formed in situ from the reaction between $[IrCl(cyclooctene)_2]_2$ and an excess of PMe_3, but the discrete complex, as far as we are aware, has not been isolated.[34] Therefore, to prepare new 11-vertex iridathiaboranes, we decided to use the PMe_3 analogue of Vaska's complex, $[IrCl(CO)(PMe_3)_2]$. Thence we have found that its reaction with Cs[*arachno*-6-SB_9H_{12}] in tetrahydrofuran (THF) solution affords the 11-vertex, pale yellow, air-stable iridathiaborane [8,8,8-$(PMe_3)_2(CO)$-*nido*-8,7-$IrSB_9H_{10}$] (**4**) in 71% yield.

The *nido*-iridathiaundecaborane cluster compound **4** was characterized by single-crystal X-ray diffraction analysis (Figure 1) and multinuclear NMR spectroscopy (Tables 1 and 2). Selected interatomic distances and angles are summarized in Table 1, together with DFT-calculated distances for the corresponding model compound [8,8,8-$(PH_3)_2(CO)$-*nido*-8,7-$IrSB_9H_{10}$] (**4a**), which represents the higher occupancy conformer. Structurally, **4** exhibits the classical 11-vertex *nido* geometry that is derived from a triangulated icosahedron by the removal of one vertex, thus conforming to the structure associated with classical electron-counting/cluster geometry paradigms.[35,36] As is quite commonly found in thiaborane clusters, the molecular structure of **4** in its crystal contains a sulfur/BH-unit disorder affecting the positions of two cluster vertices occupied by the S(7) and the BH(9) units. A complementary occupancy factor was refined, leading to S/BH occupancies of 84 and 16% for S(7). These correspond to two different conformations of the $\{Ir(CO)(PMe_3)_2\}$ vertex with respect the $\{SB_9H_{10}\}$ fragment. There are three limiting configurations of the metal coordination environment for the $\{Ir(PMe_3)_2(CO)\}$ fragment with respect to the {S(7)B(3)B(4)B(9)} face as illustrated in Scheme 1. The model of major occupancy (84%) corresponds to the conformer in which the CO ligand is *trans* to the B(9) atom (**A**), whereas in the minor disordered conformer (16%), the CO ligand is *trans* to the S(7) vertex (**B**).

The NMR data for **4** are in accord with the solid-state structure described above, and are listed in Table 2, together with its calculated nuclear magnetic chemical shielding values, DFT/GIAO calculations being performed using the B3LYP/6-31G*/LANL2DZ methodology and basis sets. These calculations were carried out to determine if the static crystalline structure corresponded to the observed ^{11}B NMR spectrum and also to aid assignment of the NMR resonances. The ^{11}B-$\{^1H\}$ NMR spectrum of **4** shows eight peaks in a 1:2:1:1:1:1:1:1 intensity ratio with the peak of relative intensity 2 resulting from an accidental overlap of two resonances. This was determined from selective ^1H-$\{^{11}B\}$ decoupling experiments which resolved two separate proton resonances and also established nine cage $^{11}B-^1H$(terminal) related pairs for the cluster BH(*exo*) units. The ^{11}B-$\{^1H\}$ NMR spectrum of this CO-ligated iridathiaborane also exhibits signals of lower intensity that indicate the minor presence of other species (vide infra). Thus, there are two bridging BHB proton resonances at $\delta(^1H) = -5.00$ and -4.18 ppm in the ^1H-$\{^{11}B\}$ spectrum with an integrated intensity ratio of 3 to 1, respectively, which may be ascribed to the presence, in solution at

(30) Kennedy, J. D. In *The Borane-Carborane-Carbocation Continuum*; Wiley: New York, 1998.
(31) Rudolph, R. W.; Pretzer, W. R. *Inorg. Synth.* **1983**, *22*, 226–231.
(32) Osborn, J. A.; Wilkinson, G. *Inorg. Synth.* **1967**, *10*, 67–71.
(33) Nestor, K.; Fontaine, X. L. R.; Greenwood, N. N.; Kennedy, J. D.; Thornton-Pett, M. *J. Chem. Soc., Dalton Trans.* **1991**, 2657–2667.
(34) Bleeke, J. R.; Haile, T.; Chiang, M. Y. *Organometallics* **1991**, *10*, 19.
(35) Williams, R. E. *Adv. Inorg. Chem. Radiochem.* **1976**, *18*, 67–142.
(36) Wade, K. *Adv. Inorg. Chem. Radiochem.* **1976**, *18*, 1–66.

Table 2. Measured ^{11}B and ^{1}H and ^{31}P NMR Data for [8,8,8-$(PMe_3)_2$(CO)-*nido*-8,7-$IrSB_9H_{10}$] (**4**), [8,8,8-$(PPh_3)_2$(CO)-*nido*-8,7-$RhSB_9H_{10}$] (**5**), and [8,8,8-(EtNC)$(PMe_3)_2$-8,7-*nido*-$IrSB_9H_{10}$] (**7**) in CD_2Cl_2 at 293 K, Compared to the Corresponding DFT/GIAO-Calculated ^{11}B-Nuclear Shielding Values for the Major Conformer **4a**, **A** in Scheme *1*, and the PMe_3 Model [8,8,8-$(PMe_3)_2$(CO)-*nido*-8,7-$RhSB_9H_{10}$] (**5a**)

	4 [**4a**]		**5** [**5a**]	**7**	
assignment[a]	$\delta(^1H)$	$\delta(^{11}B)$	$\delta(^{11}B)$	$\delta(^{11}B)$	$\delta(^1H)$
6	+5.58	+15.1[+17.0]	+15.6 [+17.0]	+12.6	+5.37
3	+3.03[b]	+0.8[c] [+9.2]	+10.1 [+11.7]	+0.7[c]	+3.34
9	+3.66	+0.8[c] [+5.6]	+9.6 [+12.2]	+0.7[c]	+3.02
4	+3.02	−1.4 [+5.4]	+4.5 [+10.3]	−3.7	+2.91
11	+3.30	−2.4 [+1.2]	+4.0 [+5.7]	−5.7	+2.88
10	+2.25	−14.4 [−14.2]	−13.8 [−11.4]	−16.0	+1.96
5	+2.25	−17.0 [−16.6]	−14.4 [−15.0]	−18.4	+1.96
1	+2.00	−26.9 [−22.7]	−18.3 [−17.3]	−27.3	+1.82
2	+1.22	−29.6 [−30.3]	−27.3 [−28.2]	−30.6	+1.20
B−H−B[d]	−5.00 (−4.18)				−5.05 (−4.11)
PMe_3	+1.86, +1.82[e]				+1.75, +1.67[f]
$MeCH_2NC$					+3.69
CH_3CH_2NC					ca. +1.6[g]
$\delta(^{31}P)$[d,h]		−27.5, −49.9[i] (−40.3[k], −49.3)		−29.1, −47.2[j] (−40.9[k], −47.1)	

[a] Assignments based on $^1H\{^{11}B\}$ selective experiments and DFT/GIAO calculated ^{11}B chemical shielding data. [b] Doublet 21 Hz, possible $^3J(^{31}P_{(1)} - {}^1H_{(3\text{ or }4)})$. [c] Accidentally coincident ^{11}B resonances. [d] Minor rotamer component in parentheses. [e] Doublets $^2J(^{31}P-^1H)$ = 9.6 and 11.0 Hz. [f] Doublets $^2J(^{31}P-^1H)$ 10 Hz. [g] Obscured by PMe_3 resonance. [h] All doublets $^2J(^{31}P-^{31}P)$ 12 Hz. [i] Measured at −50 °C. [j] Measured at −35 °C. [k] Broad, hw = 48 Hz. Compare hw ca. 33 Hz for the other ^{31}P resonances.

Scheme 1. Limiting $\{Ir(L)_2(CO)\}$-to-$\{SB_9H_{10}\}$ Conformers, and Their Relative DFT-Calculated Energies

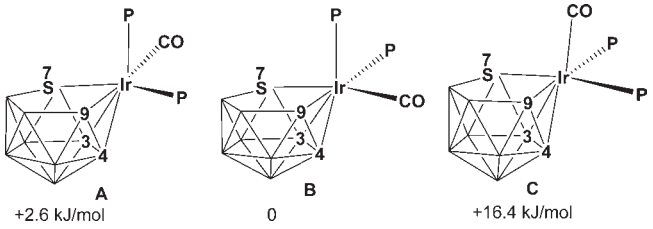

room temperature, of the two $\{Ir(L)_2(CO)\}$-to-$\{SB_9H_{10}\}$ conformers seen in the single-crystal X-ray structure. In line with this, the room temperature ^{31}P spectrum of **4** exhibits a pair of main doublets at $\delta(^{31}P)$ = −27.5 (sharp) and at −49.9 (sharp) ppm, and a minor pair at $\delta(^{31}P)$ = −40.3 (broad, doublet structure not resolved) and −49.3 (sharp) ppm. The relative intensity ratio between the major and the minor signals is about 4 to 1. The two conformers depicted in Figure 1 show that P(2) remains in a position perpendicular to the open face for both conformations, and it might be expected to exhibit a small chemical shift change in both species. In contrast, P(1) changes from a position *trans* to the sulfur-7 vertex [S(7)−Ir(8)−P(1) 165.68(5)°] to one *trans* to the boron-9 position [B(9)−Ir(8)−P(1) 160.0(9)°]. Thus, the $\{Ir(L)_2(CO)\}$-to-$\{SB_9H_{10}\}$ conformational change is expected to have a larger effect in the chemical shift of P(1) which moves upfield by −13 ppm. The broadness of this resonance may be ascribed to transoidal ^3J coupling to $^{11}B(9)$, and it exhibits a characteristic sharpening at lower temperature ($w_{1/2}$ 33 Hz at 298 K, 45 Hz at 223 K) because of thermal decoupling of the boron nucleus.[37]

The plot of $\delta(^{11}B)$ versus $\delta(^1H)$ shows that there is an approximately linear correlation for directly bound $[BH_t]$ units in both of the metallathiaboranes (see Supporting Information). Overall, the *exo*-hydrogen atoms in **4** are deshielded with respect those of **6**, with the principal deviation occurring at the BH(6) position antipodal to the metal, for which the resonance of the terminal hydrogen atom shifts significantly toward lower field (ca. 1.8 ppm) when the atom is Ir. This anomalously low proton shielding for *exo*-terminal protons has been previously noted in 12-vertex *closo*-metallaheteroboranes,[38−42] being considered as diagnostic of an antipodal third-row transition-element center, a diagnostic that now can be also invoked in 11-vertex *nido*-metallathiaborane systems.

The BHB proton resonances in **4** are shifted toward higher field with respect to the value found for the [8,8,8-$(PPh_3)_2$-(CO)-*nido*-8,7-$RhSB_9H_{10}$] (**5**) analogue.[43] The chemical shift of the bridging hydrogen atom on the pentagonal open face of 11-vertex *nido*-rhodathiaboranes is particularly sensitive to the number and nature of the *exo*-polyhedral ligands bound to the metal center, and it has been proposed that a higher-field shift of the BHB proton resonance correlates with a negative charge buildup on the metal center in 11-vertex *nido*-metallathiaboranes.[44] The superior σ-donor character of the PMe_3 ligands relative to the PPh_3 ligands could, therefore, perhaps be invoked as a principal factor in the observed shift of the bridging hydrogen resonance to higher fields.

Overall, there are no large and distinctive differences between the calculated boron nuclear shieldings of the three PMe_3-ligated conformers of **4** in Scheme 1 (only the calculated

(37) Beall, H.; Bushweller, C. H.; Dewkett, W. J.; Grace, M. *J. Am. Chem. Soc*. **1970**, *92*, 3484.

(38) Ferguson, G.; Gallagher, J. F.; McGrath, M.; Sheehan, J. P.; Spalding, T. R.; Kennedy, J. D. *J. Chem. Soc., Dalton Trans*. **1993**, 27.

(39) Faridoon; Dhubhghaill, N. O.; Spalding, T. R.; Ferguson, G.; Kaitner, B.; Fontaine, X. L. R.; Kennedy, J. D. *J. Chem. Soc., Dalton Trans*. **1989**, 1657–1668.

(40) Ferguson, G.; Kennedy, J. D.; Fontaine, X. L. R.; Faridoon; Spalding, T. R. *J. Chem. Soc., Dalton Trans*. **1988**, 2555–2564.

(41) Faridoon; Dhubhghaill, O. N.; Spalding, T. R.; Ferguson, G.; Kaitner, B.; Fontaine, X. L. R.; Kennedy, J. D.; Reed, D. *J. Chem. Soc., Dalton Trans*. **1988**, 2739–2745.

(42) Ferguson, G.; Parvez, M.; MacCurtain, J. A.; Dhubhghaill, O. N.; Spalding, T. R.; Reed, D. *J. Chem. Soc., Dalton Trans*. **1987**, 699–704.

(43) Coughlan, S.; Spalding, T. R.; Ferguson, G.; Gallagher, J. F.; Lough, A. J.; Fontaine, X. L. R.; Kennedy, J. D.; Štíbr, B. *J. Chem. Soc., Dalton Trans*. **1992**, 2865–2871.

(44) Álvarez, A.; Macías, R.; Fabra, M. J.; Martín, M. L.; Lahoz, F. J.; Oro, L. A. *Inorg. Chem*. **2007**, *46*, 6811–6826.

data for the major component, **A**, are given in Tables 1 and 2, the data for the others can be found in the Supporting Information). There are, however, significant discrepancies between these calculated values and those observed experimentally. A consequence here is that there is a degree of uncertainty in the spectroscopic assignment, in compound **4**, of the boron atoms B(3), B(4), and B(9) that are directly connected to the Ir(8) atom, as well as of the B(11) atom bound to the S(7) vertex. For the B(3) and B(9) atoms, the deviations between the calculated nuclear shielding and those measured experimentally are within about 8 ppm; whereas for the atoms B(1) to B(6), which form the lower-belt pentagonal pyramid, and for the B(10) atom, connected exclusively to boron atoms, the agreement is more satisfactory. Thus, the principal deviations between experimental and calculated shielding values were for the boron atoms directly bound to the iridium center.

According to the DFT-calculated energies, the molecule with the CO ligand *trans* to the S(7) vertex (schematic **B** above) is the conformer of lowest energy, followed successively (i) by the rotamer with the CO ligand in the position *trans* to the B(9) atom (2.6 kJ/mol higher; schematic **A**), and (ii) by the rotamer with the CO ligand *trans* to the B(3)−B(4) edge (16.4 kJ/mol higher; schematic **C**). These differences are small, and can readily be obscured by solvent and/or packing-force interactions, suggesting that the conformers may be in dynamic equilibrium in solution. However, variable temperature NMR experiments between room temperature and 120 °C did not reveal interconversion between the conformers. This indicates that the transition state energy of a {Ir(L)$_2$(CO)}-to-{SB$_9$H$_{10}$} conformation in this system is relative high.

On the other hand, it is interesting to note that the observed boron chemical shifts reported for the PPh$_3$ rhodathiaborane **5** match better the values calculated for the PMe$_3$ iridathiaborane conformers, **A**, **B**, and **C** (Scheme 1) than those found for the iridathiaborane analogue, **4**. This observation suggests that the B3LYP methodology (with the 6-31G* and LANL2DZ basis-sets) used in the calculation underestimates the contribution of the iridium atom to the shielding of the boron vertices. Nevertheless, the ^{11}B chemical shifts calculated for the PMe$_3$ conformers reproduce the experimental trend, and they are sufficiently in agreement to propose the assignments listed in Table 2.

The clusters in the new iridathiaborane **4**, and its rhodathiaborane analogue **5**, in which the metal-atom vertices can be considered to be formally Ir(III) or Rh(III), are examples of 11-vertex, 13-skeletal-electron-pair (sep), clusters that conform to the Wade/Mingos approach.[36,45] However, the parent rhodathiaborane, [8,8-(PPh$_3$)$_2$-*nido*-8,7-RhSB$_9$H$_{10}$] (**3**), with one *exo*-polyhedral ligand fewer and what can be formally considered as a Rh(I) center, would have a 12-sep cluster count and would therefore not conform to the electron counting formalism, being formally unsaturated with respect **4** and **5**. The origins of this apparent inconsistency reside in the ready propensity of rhodium centers to switch between formally square-planar Rh(I) and formally octahedral Rh(III). This has been adequately discussed elsewhere, for both the Rh(I)/Rh(III) and the related Pt(II)/Pt(IV) behaviors.[23,30]

(45) Mingos, D. M. P.; Wales, D. J. *Introduction to Cluster Chemistry*; Prentice Hall: London, 1990.

Scheme 2

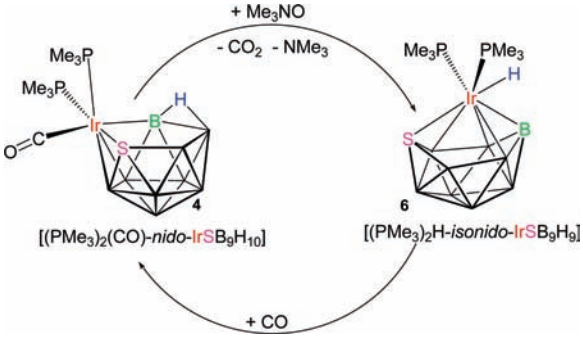

In any event, the removal of one of the three *exo*-polyhedral metal-bound ligands in **4** would lead to an iridathiaborane that would be isoelectronic, in terms of bonding-electron cluster count, with the interestingly reactive rhodathiaborane **3** mentioned in the introduction. Such a removal would afford the opportunity to study the influence that the metal may have in altering the reactivity of the 11-vertex MSB$_9$ system based on **3**. In accord with this idea, we have found that treatment of compound **4** with the decarbonylating agent Me$_3$NO in dichloromethane removes the CO ligand. The product now, however, is the new iridathiaborane, [1,1,1-(PMe$_3$)$_2$(H)-*isonido*-1,2-IrSB$_9$H$_9$] (**6**), formed in high yield (Scheme 2), rather than its structured isomer [8,8-(PPh$_3$)$_2$-*nido*-8,7-IrSB$_9$H$_{10}$], the iridium analogue of the rhodathiaboranes **3**.

Compound **6** was studied by a single-crystal X-ray diffraction analysis, which revealed a static disorder involving the Ir(1), S(7), and B(3) vertices. Thus, it was found that these atoms were in two possible positions in the cluster, and the model for the disorder assumed, therefore, the exchange of the Ir(1) atom between those two positions, together with the concomitant mutual exchange of the S(2) and B(3) atoms with two very different complementary occupancy factors of 88 and 12%. The result of this analysis, illustrated in Figure 2, is two clusters related by a 180° rotation around an axis that passes through the Ir(1) vertex and the B(10)−B(11) edge. The iridium-bound hydrogen atom was included in the last cycles of refinement, with a light positional restraint, from an XHYDEX electrostatic potential well calculation,[46,47] but only for the model of major occupancy [Figure 2 (a)] (for details, see the Supporting Information for this paper).

The restraints set to deal with the disorder imply a loss of precision in some of the distances and angles of the cluster. Nevertheless, the crystallographic data reasonably allow the unequivocal determination of the structure of **6**. The "long" distance between the Ir(1) and B(4) atoms, of 2.779(9) Å in the higher occupancy molecule, and of 2.763(11) Å in the molecule of lower occupancy, renders a quadrilateral open face that is reminiscent of the series of *isonido* 11-vertex clusters that have been previously reported in the literature.[48−52]

(46) Orpen, A. G. *J. Chem. Soc., Dalton Trans.* **1980**, 2509–2516.
(47) Farrugia, L. J. *J. Appl. Crystallogr.* **1999**, *32*, 837–838.
(48) Volkov, O.; Macías, R.; Rath, N. P.; Barton, L. *J. Organomet. Chem.* **2002**, *657*, 40–47.
(49) Bown, M.; Fontaine, X. L. R.; Greenwood, N. N.; Kennedy, J. D.; Thornton-Pett, M. *Organometallics* **1987**, *6*, 2254–2255.
(50) Nestor, K.; Fontaine, X. L. R.; Greenwood, N. N.; Kennedy, J. D.; Plešek, J.; Štíbr, B.; Thornton-Pett, M. *Inorg. Chem.* **1989**, *28*, 2219–2221.
(51) Bould, J.; Rath, N. P.; Barton, L. *Acta. Crystallogr. Sect. C* **1997**, *53*, 416–419.

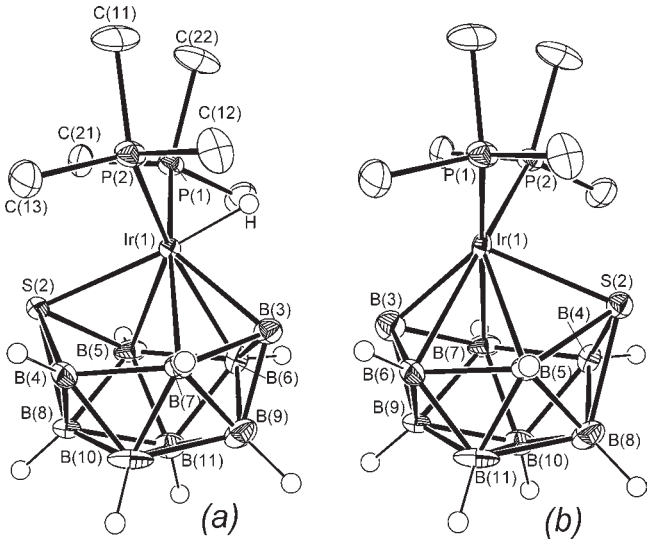

Figure 2. ORTEP-type drawings of the crystallographically determined structures of (a) the major (88%) and (b) the minor (12%) occupancy conformers of **6**, with 50% probability ellipsoids. Hydrogen atoms on the PMe_3 ligands are omitted to aid clarity. The iridium-bound hydrogen atom in (a) derives from XHYDEX calculations; the same procedure was not carried out for (b), and so the iridium-bound hydrogen atom is omitted.

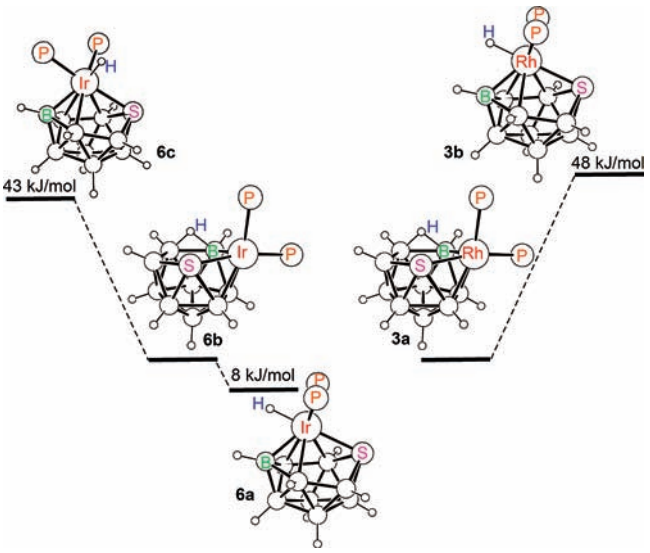

Figure 3. DFT-calculated energies and structures, computed at the B3LYP/6-31G*/LANL2DZ level for the PMe_3-ligated *nido*- and *isonido*-iridathiaborane isomers, $[(PMe_3)_2HIrSB_9H_9]$ (left), and for the rhodathiaborane counterparts on the PH_3 models $[(PH_3)_2RhSB_9H_{10}]$ (right).

This structural feature relates to the fluxional behavior found in the *nido*-rhodathiaborane $[(PPh_3)_2RhSB_9H_{10}]$ **3** that leads to the exchange of the enantiomeric forms of the cluster.[27] DFT-calculations on the $[(PH_3)_2RhSB_9H_{10}]$ **3a** model for **3** suggested that the fluxional process takes place through 11-vertex *isonido*-intermediates. The observed structure of **6**, therefore, supports these DFT findings for the rhodathiaborane system, and it provides further experimental incidence of structures in the 11-vertex *nido-isonido-closo* structural continuum.

The inclusion of an iridium vertex in the $\{MSB_9\}$ cluster now offers a clear example on structural control by the metal center in 11-vertex metallaheteroboranes: in compound **6** the $\{IrH(PMe_3)_2\}$ fragment stabilizes a hydride-ligated *isonido*-cluster instead of the BHB hydrogen-bridged *nido*-structure that is found for the rhodathiaborane analogue **3**. DFT calculations for compound **6** reproduce these experimental results and provide further information for the comparison of rhodium versus iridium (Figure 3). Hence, in the iridathiaborane system, the energy of the *nido*-isomer, **6b** in Figure 3, lies only 8 kJ/mol higher in energy than the *isonido*-structure, **6a** in Figure 3; whereas, in the $[(PH_3)_2RhSB_9H_{10}]$ models, **3a** and **3b** in Figure 3, the DFT-calculated energy of the *nido* cluster is 48 kJ/mol lower in energy.[27] Thus, when compared with the $\{Rh(PH_3)_2\}$-fragment, the iridium has the effects (a) of reducing the energy difference between the two limiting structures and (b) of reversing the observed relative stability of the isomers.

Examination of the optimized structure for **6a**, which conforms to the structure determined for the major component by the X-ray analysis, reveals that the hydride ligand is *trans* to the S(2) vertex, with an H−Ir(1)−S(2) angle of 177°. Interestingly, an $IrH(PMe_3)$-to-SB_9H_9 rotation leads to a local energy minimum in the DFT calculation, now with an H−Ir(1)−S(2) angle of 83°, giving a second *isonido* conformer **6c** that lies 43 kJ/mol above the *trans*-isomer **6a**. Although the *trans*-effect of hydride ligands in complexes of iridium is well documented, it is somewhat surprising to find that a simple metal-to-thiaborane conformational change results in such a large increase in the DFT-calculated energy of the system. It is clear that there is a preference of the hydride ligand to occupy the position *trans* to the sulfur atom and that this effect is playing an important role in stabilizing the *isonido* structure versus the *nido*.

Thus, although the calculated energy difference between the *nido* and the *isonido* clusters is only 8 kJ/mol, suggesting a potential *nido* ↔ *isonido* equilibrium and/or fluxional processes in solution, the barrier for the conversion of the H-ligated *isonido*-cluster to the BHB hydrogen bridged *nido* structure through $Ir(L)_2$-to-SB_9 conformational changes, appears to be high in energy, precluding the formation of measurable amounts of the *nido*-iridathiaborane isomer at room temperature. This appears to hold at temperatures above the ambient one (for example 80 °C in toluene), at which the NMR spectra of **6** reveal only the presence of the hydridoiridathiaborane, which exhibits patterns in the ^{11}B

Table 3. Measured ^{11}B, ^1H and ^{31}P NMR Data for Compound [1,1,1-H$(PMe_3)_2$-1,2-*isonido*-$IrSB_9H_9$] (**6**), CD_2Cl_2 Solution at 293 K, Together with DFT-Calculated Boron Nuclear Shielding Data

assignment[a]	DFT-calcd $\delta(^{11}B)$[b]	$\delta(^{11}B)$ [^1J(B,H)/Hz]	$\delta(^1H)$
3	+52.1	+44.9 [164]	+6.61
9	+22.8	+24.6 [137]	+5.59
4, 5	+12.2,+12.1	+7.6(2) [143]	+2.63
8	−17.5	−13.5 [158]	+2.45
6,7	−12.1, −28.5 [−20.3]	−25.9(2) [145]	−0.77
10,11	−12.8, −28.7 [−20.8]	−28.4(2) [143]	−0.74
Ir−*H*			−9.03[c]
PMe_3			+1.63[d]
$\delta(^{31}P)$ (−50 °C)		−45.1	

[a] Assignments based on ^{11}B-{^1H selective decoupling} experiments in combination with DFT/GIAO calculated ^{11}B chemical shielding data. [b] Values [in brackets] are the average of the measured chemical shifts for two equivalent sites. [c] Triplet ^2J ($^{31}P - {}^1H$) 21 Hz. [d] Doublet ^2J ($^{31}P - {}^1H$) 9 Hz.

(52) Bown, M.; Grüner, B.; Štíbr, B.; Fontaine, X. L. R.; Thornton-Pett, M.; Kennedy, J. D. *J. Organomet. Chem.* **2000**, *614*, 269–282.

Scheme 3. Proposed Mechanism for the Fluxional Behavior of **6** in Solution

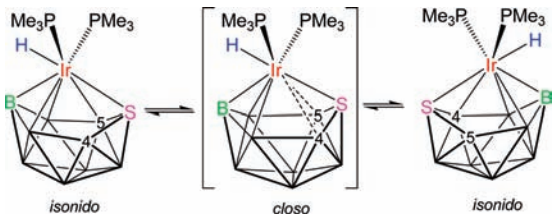

and $^{31}P\{^{1}H\}$ NMR spectra in solution (Table 3) that agree with an 11-vertex *closo*-structure, indicating that the *isonido*-cluster is undergoing a dynamic process that renders the two PMe_3 ligands equivalent in addition to the corresponding pairs of boron vertices. These NMR data, therefore, contrast with the asymmetric *isonido*-structure found in the solid state of the iridathiaborane and its calculated PMe_3 model.

A *nido*-structured isomer of **6** could be an intermediate in the observed stereochemical non-rigidity of **6** at room temperature. However, the energy trend calculated for the three isomers, **6a**, **6b**, and **6c**, suggests that the 11-vertex iridathiaborane system, in its *isonido*−*isonido* transformation in solution, follows a pathway of lower activation energy. A possible mechanism for the fluxional process, could be a simple lengthening of the Ir(1)−B(5) connection and shortening of the Ir−B(4) link via a *closo* structure (Scheme 3).

On the other hand, the above-commented non-rigidity suggests that the cluster could open coordination sites at the iridium center and thus make **6** a reactive species. This hypothesis is confirmed by the reactions of **6** with CO and EtNC, which respectively lead to the quantitative reformation of **4** and to the new EtNC-ligated iridathiaborane, [8,8,8-$(PMe_3)_2$(CNEt)-*nido*-8,7-$IrSB_9H_{10}$] (**7**). Solutions of **6** at about 300 K, under a CO atmosphere, when monitored by ^{11}B NMR spectroscopy, show a slow uptake of the CO over a period of 2 h to afford **4**, with the spectrum again showing the presence of the minor component. In turn, heating of **4** in refluxing toluene regenerates **6**, although in practice the oxidative removal of CO by Me_3NO is more convenient. Thus, the regeneration of the CO-ligated cluster results in a stoichiometric cycle (Scheme 2), which illustrates the *nido*-to-*isonido* flexibility of this system. Reaction with EtNC is, however, much slower and requires heating of solutions in toluene with a hot-air gun to effect reaction. On cooling, colorless crystals form and a 93% isolated yield of **7** may be obtained.

Compound **7** was characterized by NMR experiments and by a single-crystal X-ray diffraction analysis (Figure 4, Tables 1 and 2). The crystallographically obtained molecular structure exhibits the same kind of positional disorder between the B(9) and S(7) vertices as for the CO-ligated counterpart **4**. For **7**, this static molecular disorder involves two different {η^4-SB_9H_{10}}-to-{Ir(CNEt)$(PMe_3)_2$} conformations with complementary occupation factors of 86 and 14%, corresponding to the EtNC ligand being *trans* either to the B(9) atom or to the S(7) vertex, respectively. The Oak Ridge thermal ellipsoid plot (ORTEP)-type of drawing in Figure 4 shows the structure of the isomer with the higher occupancy factor, and the geometrical parameters in Table 1 also refer to this isomer (see the Supporting Information for the structural data for the minor conformer). This major conformer of the EtNC compound **7** exhibits the same type of thiaborane-to-iridium coordination as the CO-ligated analogue **4**, with the EtNC and CO ligands each occupying the position *trans* to the B(9) vertex. Overall, there are no significant differences among the distances and the angles within the two {$IrSB_9H_{10}$} clusters of **4** and **7**, although the Ir−B(9) distance appears to be somewhat longer in **7**, at 2.35(2) Å, than in **4**, at 2.273(16) Å, suggesting a higher *trans* effect of the isocyanide ligand compared with carbonyl.

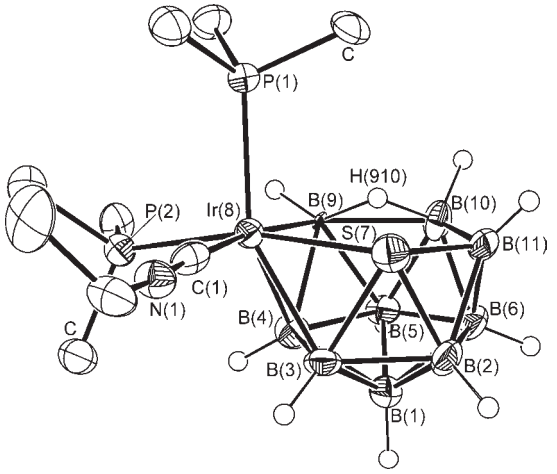

Figure 4. ORTEP-type drawing of the crystallographically determined molecular structure of the major occupancy conformer of **7** with 50% probability ellipsoids. Hydrogen atoms on the organic ligands are omitted to aid clarity.

The NMR data for **7** agree with the asymmetric structure found by the X-ray diffraction analysis and are very similar to the data for the CO-ligated analogue **4** (Table 2). The ^{11}B NMR spectrum of **7** features eight signals, with a relative intensity pattern of 1:2:1:1:1:1:1:1, which are slightly shielded, with a mean $\delta(^{11}B)$ value of about −10 ppm compared to the resonances of the CO analogue **4**, which have a mean $\delta(^{11}B)$ value of −8 ppm. This increased shielding may be due to the higher σ-donor character and lower π-basicity of the EtNC versus the CO ligand, which provide the iridium center with better electron-donating capabilities that result in a higher electron density delocalized over the thiaborane framework, and which leads to the observed net shielding increase for the boron nuclei. As with **4**, the peak of double intensity corresponds to two accidentally coincident resonances, as shown by ^{1}H-{^{11}B(selective decoupling)} experiments which resolve two separate proton signals. Again as with **4**, the high-field region of the ^{1}H-{^{11}B} spectrum of **7** features two resonances, now at −5.10 and −4.17 ppm, of 86:14 relative intensity, respectively, corresponding to the BHB bridging hydrogen atoms of the two rotamers, analogous to those for the CO compound. Thus, two different conformations of the {Ir$(PMe_3)_2$(EtNC)} fragment with respect to the {S(7)B(3)B(4)B(9)} face are present in solution at room temperature, suggesting that the energy differences among the possible limiting conformers is small, as with compound **4** (see schematics **A**, **B**, and **C** above) . This feature contrasts with the higher difference in energy calculated for the {Ir$(PMe_3)_2$(H)}-to-{SB_9} conformational change in the 11-vertex iridathiaborane system, discussed above.

Conclusions

In contrast to PPh_3-ligated Vaska's compound [IrCl(CO)-$(PPh_3)_2$], which shows no reaction with the $[SB_9H_{12}]^-$ anion,

Table 4. Experimental X-ray Diffraction Parameters and Crystal Data for $[(PMe_3)_2(CO)$-*nido*-$IrSB_9H_{10}]$ **4**, $[(PMe_3)_2H$-*isonido*-$IrSB_9H_9]$ **6**, and $[(PMe_3)_2(EtNC)$-*nido*-$IrSB_9H_{10}]$ **7**

	4	**6**	**7**
empirical formula	$C_7H_{28}B_9IrOP_2S$	$C_6H_{28}B_9IrP_2S$	$C_9H_{33}B_9IrNP_2S$
mol. wt.	511.78	483.77	538.85
cryst dimens (mm)	0.07 × 0.17× 0.28	0.08 × 0.08× 0.20	0.06 × 0.17× 0.20
crystal system	monoclinic	monoclinic	orthorhombic
space group	$P_{2_1/n}$	$P_{2_1/n}$	C_{2221}
a, Å	8.7688(16)	9.1310(18)	14.6629(12)
b, Å	16.490(3)	14.686(3)	15.0013(12)
c, Å	13.619(3)	13.314(3)	19.9118(17)
β, deg	98.649(3)	92.848(3)	
V, Å^3	1946.9(7)	1783.2(6)	4379.9(6)
Z	4	4	8
D(calcd) g cm^{-3}	1.746	1.798	1.634
μ(Mo K$_\alpha$) mm^{-1}	7.118	7.761	6.330
temperature, K	100(2)	100(2)	150(2)
$2\theta_{max}$, deg	56.6	56.8	55.5
transmission factors	0.2423, 0.6548	0.3059, 0.5756	0.3641, 0.7026
no. of rflns collected	12833	21630	25225
no. of indp rflns	4625	4311	5076
no. of rflns obsd ($I > 2\sigma(I)$)	3964	4203	4507
no. of params refined	197	200	225
R	0.0349	0.0487	0.0385
R_w	0.0850	0.1075	0.0864
goodness of fit	1.07	1.48	1.05

$[IrCl(CO)(PMe_3)_2]$ undergoes a simple metathetical reaction and acts as a source of the $\{Ir(CO)(PMe_3)_2\}$ fragment leading to the formation of the new 11-vertex iridathiaborane, $[8,8,8$-$(CO)(PMe_3)_2$-*nido*-$8,7$-$IrSB_9H_{10}]$ (**4**) in good yield. A mixture of two $\{Ir(CO)(PMe_3)_2\}$-to-$\{SB_9H_{10}\}$ conformers is found, both in solution and in the solid state, and although DFT-calculations on the $[(CO)(PMe_3)_2IrSB_9H_{10}]$ conformers indicate that the energy difference is small, the large difference in the ratios found in solution suggests that the activation energy of conversion between the conformers is high, precluding a dynamic equilibrium of the species at room temperature.

The decarbonylation of **4** has allowed the preparation of 11-vertex $[1,1,1$-$(PMe_3)_2(H)$-*isonido*-$1,2$-$IrSB_9H_9]$ (**6**), of which the *isonido* metallathiaborane cluster unit, according to electron-counting rules, is isoelectronic with the *nido* structure of the rhodathiaborane $[8,8,8$-$(PPh_3)_2$-*nido*-$8,7$-$RhSB_9H_{10}]$ (**3**). The structural differences between the two compounds constitute an interesting demonstration of tuning and control of metallaheteroborane cluster structure by choice of metal center. In the previously reported analogous rhodathiaborane system, the energy of the cluster increases in the order, *nido*→*isonido*→*closo*, whereas the incorporation of iridium into the system reverses this energy continuum, stabilizing the *isonido* cluster over the *nido*. In the *isonido* hydridoiridathiaborane, **6**, the $\{Ir(H)(PMe_3)_2\}$ vertex can be regarded as a donor of two electrons to the cluster framework; thereby exhibiting the higher oxidation state of iridium(III), in contrast to the *nido*-configuration of **3**, where the $\{Rh(PPh_3)_2\}$ fragment formally donates one electron, and is formally rhodium(I). Higher oxidation states are comparatively more stable for iridium than for rhodium, and iridium hydrido compounds are also particularly stable; these two factors can play an important role in the stabilization of the Ir-hydrogen-ligated iridium(III) *isonido*-hydridoiridathiaborane **6** versus the rhodium(I) *nido* species **3** in which the hydrogen atom prefers to occupy a BHB bridging position.

The hydridoiridathiaborane **6** is very fluxional in solution, implying a ready cluster opening to *nido* for potential access to a reactive metal center. Thus, *isonido* **6** reacts with Lewis bases such as CO, which regenerates *nido* **4**, or with EtNC, which generates a structural analogue of **4**, demonstrating a *nido*-to-*isonido* flexibility that augurs for a rich chemistry to complement and extend, for example, the recent reported reactivity[13−15] of pyridine-ligated rhodathiaborane with unsaturated organic molecules.

Experimental Section

General Procedures. Reactions were carried out under an argon atmosphere using standard Schlenk-line techniques. Solvents were dried by standard techniques and transferred to reaction vessels either by bulb-to-bulb condensation or by injection via syringe. All commercial reagents were used as received without further purification. EtNC was prepared according to the literature method. The 10-vertex *arachno*-thiaborane salt, $Cs[arachno$-6-$SB_9H_{12}]$,[31] $[IrCl(CO)(PMe_3)_2]$,[53] EtNC,[54] and $[(PPh_3)_2RhSB_9H_{10}]$[25] were prepared essentially according to the literature methods. Preparative thin-layer chromatography (TLC) was carried out using 1 mm layers of silca gel G (Fluka, type GF254) made from water slurries on glass pates of dimensions 20 × 20 cm and dried in air at 25 °C. Infrared spectra were recorded on a Perkin-Elmer Spectrum 100 spectrometer, using an Universal ATR Sampling Accessory. NMR spectra were recorded on Bruker Avance 300-MHz and AV 400-MHz spectrometers or a Varian MERCURY 400 High Resolution System, using ^{11}B, ^{11}B-$\{^1H\}$, ^1H, ^1H-$\{^{11}B\}$, and ^1H-$\{^{11}B$(selective)$\}$ techniques. ^1H NMR chemical shifts were measured relative to partially deuterated solvent peaks but are reported in parts per million (ppm) relative to tetramethylsilane. ^{11}B chemical shifts are quoted relative to $[BF_3(OEt)_2]$, and ^{31}P chemical shifts are quoted relative to 85% aqueous H_3PO_4. Mass spectrometric data were recorded on a VG Autospec double-focusing mass spectrometer, on a microflex MALDI-TOF, and on a ESQUIRE 3000+ API-TRAP, operating in either positive or negative modes.

Synthesis of $[8,8,8$-$(CO)(PMe_3)_2$-$8,7$-*nido*-$IrSB_9H_{10}]$ (4). Tetrahydrofuran (thf, 18 mL) was injected via a septum into a two-neck flask containing an argon atmosphere, a stir bar,

(53) Labinger, J. A.; Osborn, J. A. *Inorg. Synth.* **1983**, *18*, 62–65.
(54) Jackson, H. L.; McKusic, B. C. *Org. Synth.* **1955**, *35*, 62–64.

[IrCl(CO)(PMe_3)$_2$] (53 mg, 0.13 mmol), and Cs [*arachno*-SB_9H_{12}] (37 mg, 0.135 mmol). After stirring for 5 days, the flask was opened to the atmosphere, and the fine white precipitate removed by filtration and washed with thf. The filtrate was reduced in volume on a rotary evaporator, applied to preparative TLC plates and developed with CH_2Cl_2/hexane 80:20. Two bands were observed under UV illumination, a weak band at R_F 0.7, and a main band at R_F 0.4 containing the product **4** (46.9 mg, 0.092 mmol, 71%). IR/cm^{-1} ν(C≡O) 2015s (major conformer), 1969sh (minor conformer); ν(B−H) 2510, 2551. Anal. Calcd. for $C_7H_{28}B_9P_2Ir_1S_1O_1$: C, 16.43; H, 5.51; S, 6.26. Found: C, 16.48; H, 5.41; S, 6.54. The mass spectrum shows an isotopomer envelope at 484 with intensities corresponding to those calculated for **4** with loss of CO, namely, $C_6H_{28}B_9P_2IrS$. The compound was crystallized from CH_2Cl_2/hexane solution. NMR data are listed in Table 2.

Synthesis of [1,1,1-(H)(PMe_3)$_2$-1,2-*isonido*-$IrSB_9H_9$] (6). Method A. [(CO)(PMe_3)$_2$$IrSB_9H_{10}$] (**4**, 48.6 mg, 94.6 μmol) and $Me_3NO\cdot 2H_2O$ (11.1 mg, 100 μmol) were placed in a round-bottom flask. Dichloromethane, about 10 mL, was condensed at liquid-nitrogen temperature, and the mixture allowed to warm to room temperature with stirring. Monitoring by ^{11}B NMR spectroscopy showed complete conversion to the title compound **6**. The solvent was pumped off on the Schlenk line, and the compound washed out with a minimum of Et_2O, giving a pale lemon-yellow powder (40.3 mg, 83.3 μmol, 88%). IR/cm^{-1} ν(Ir−H) 2197; ν(B−H) 2569, 2524, 2500. Anal. Calcd. for $C_6H_{28}B_9P_2Ir_1S_1$: C, 14.90; H, 5.83; S, 6.63. Found: C, 15.10; H, 5.14; S, 5.69. NMR data are listed in Table 4.

Method B. Smaller amounts of compound **6**, suitable for further in situ experiments, may also be obtained by the heating of solutions of **4** in toluene in air, in a capped NMR tube, with a concomitant monitoring of the progress of the decarbonylation by ^{11}B NMR spectroscopy.

Crystals of **6** for single-crystal X-ray crystallography were grown via diffusion of hexane through a layer of benzene into a solution of the compound in CH_2Cl_2. They may also be grown from hot solution in toluene.

Synthesis of [8,8,8-(EtNC)(PMe_3)$_2$-8,7-*nido*-$IrSB_9H_{10}$] (7). [H(PMe_3)$_2$-*isonido*-$IrSB_9H_9$] (**6**, 2.0 mg, 4 μmol) was placed in an NMR tube equipped with a Teflon screw valve and $CD_3C_6D_5$ (ca. 0.7 mL) added. The tube was attached to the Schlenk line, the air evacuated, and an excess amount of EtNC condensed in. The tube was sealed and warmed with a heat gun. The mixture initially rapidly went yellow as compound **6** dissolved, and then very quickly became colorless. At this point ^{11}B NMR spectroscopy showed complete conversion to a single component, subsequently identified as [7,7,7-(EtNC)(PMe_3)$_2$-7,11-*nido*-$IrSB_9H_{10}$] (**7**). The tube was left in the freezer overnight, and next day the semicrystalline product **7** (2.0 mg, 3.7 μmol, 93%) was washed out of the tube. IR/cm^{-1} ν(NC) 2179; ν(B−H) 2519, 2503, 2491. Single crystals suitable for X-ray analysis were obtained by diffusion of hexane through a small layer of benzene into a solution of the compound in CD_2Cl_2. Anal. Calcd for $C_9H_{33}B_9P_2Ir_1N_1S_1$: C, 20.06; H, 6.17; S, 5.95. Found: C, 20.66; H, 6.17; S, 5.56. NMR data are listed in Table 2.

X-ray crystallography. Data for compounds **4** and **6** were collected on a Bruker SMART APEX CCD system, and those for **7** on a Bruker Nonius CCD diffractometer with a FR591 rotating-anode generator. The structures were solved and refined using the programs and SHELXL-97,[55,56] respectively. The programs ORTEP-3[47] and PLATON[57] were used to prepare the figures and the crystallographic data gathered in the Supporting Information. Salient crystallographic collection data and derived molecular dimensions are summarized in Tables 1 and 4.

Calculations. All calculations were performed using the Gaussian 03 package[58] Structures were initially optimized using standard methods with the STO-3G* basis-sets for B, P, S, and H with the LANL2DZ basis-set for the metal atom. The final optimizations, including frequency analyses to confirm the true minima, together with GIAO NMR nuclear-shielding predictions, were performed using B3LYP methodology, with the 6-31G* and LANL2DZ basis-sets. GIAO NMR nuclear shielding predictions were performed on the final optimized geometries, and computed ^{11}B shielding values were related to chemical shifts by comparison with the computed value for B_2H_6 which was taken to be δ(^{11}B) +16.6 ppm relative to the $BF_3(OEt_2)$ = 0.0 ppm standard. In each case the compounds were modeled using hydrogen atoms rather than methyl and phenyl groups on the phosphine ligands to reduce computation time.

Acknowledgment. We acknowledge the Spanish Ministry of Science and Innovation (CTQ2009-10132, CONSOLIDER INGENIO, CSD2009-00050, MULTICAT and CSD2006-0015, Crystallization Factory) for support of this work. R.M. thanks the MEC-Universidad de Zaragoza and the European Social Fund for his Research Contract in the framework of the "Ramón y Cajal" Program. J.B. was supported by the Diputación General de Zaragoza and Caja Inmaculada (Grant CB5/09); and, in part, by the Grant Agency of the Czech Republic, project no. 203/06/P398 and the Grant Agency of the Academy of Sciences of the Czech Republic, project no. IAA400320601.

Supporting Information Available: Additional information in the form of tables and figures and crystallographic data in CIF format. This material is available free of charge via the Internet at http://pubs.acs.org.

(55) Sheldrick, G. M.; *SADABS, Program for Correction of Area Detector Data*; Univerisity of Göttingen: Göttingen, Germany, 1999.

(56) Sheldrick, G. M. *SHELXL-97*; University of Göttingen: Göttingen, Germany, 1997.

(57) Spek, A. L. *J. Appl. Crystallogr.* **2003**, *36*, 7–13.

(58) Frisch, M. J.; Trucks, G. W.; Schlegel, H. B.; Scuseria, G. E.; Robb, M. A.; ; Cheeseman, J. R.; Jr., J., A. M.; Vreven, T.; Kudin, K. N.; Burant, J. C.; J. M..Millam; Iyengar, S. S.; Tomasi, J.; Barone, V.; Mennucci, B.; ; Cossi, M.; Scalmani, G.; Rega, N.; Petersson, G. A.; Nakatsuji, H.; Hada, M.; Ehara, M.; Toyota, K.; Fukuda, R.; Hasegawa, J.; Ishida, M.; Nakajima, T.; Honda, Y.; Kitao, O.; Nakai, H.; Klene, M.; Li, X.; Knox, J. E.; Hratchian, H. P.; Cross, J. B.; Bakken, V.; Adamo, C.; Jaramillo, J.; ; Gomperts, R.; Stratmann, R. E.; Yazyev, O.; Austin, A. J.; Cammi, R.; ; Pomelli, C.; Ochterski, J.; Ayala, P. Y.; Morokuma, K.; Voth, G. A.; Salvador, P.; Dannenberg, J. J.; Zakrzewski, V. G.; Dapprich, S.; Daniels, A. D.; Strain, M. C.; Farkas, O.; Malick, D. K.; Rabuck, A. D.; Raghavachari, K.; Foresman, J. B.; Ortiz, J. V.; Cui, Q.; Baboul, A. G.; Clifford, S.; Cioslowski, J.; Stefanov, B. B.; Liu, G.; Liashenko, A.; Piskorz, P.; ; Komaromi, I.; L.Martin, R.; Fox, D. J.; Keith, T.; Al-Laham, M. A.; Peng, C. Y.; Nanayakkara, A.; Challacombe, M.; Gill, P. M. W.; Johnson, B. G.; Chen, W.; Wong, M. W.; Gonzalez, C.; Pople, J. A. *Gaussian 03*; Gaussian, Inc: Wallingford, CT, 2004.